COMPACT DUAL-BAND DUAL-RING PRINTED MONO-POLE ANTENNAS FOR WLAN APPLICATIONS

K. H. Sayidmarie[*] and T. A. Nagem

Department of Communication Engineering, College of Electronic Engineering, University of Mosul, Iraq

Abstract—Three dual band planar monopole antennas for wireless local area network (WLAN) application are proposed. The antennas have common configuration in the form of rectangular, rhombic and annular double rings. All the antennas use the self similarity property to exhibit dual band characteristics. The proposed antennas cover the frequency bands of the IEEE 802.11 a/b/g (2.4–2.48 GHz, 5.15–5.35 GHz and 5.725–5.825 GHz), and have radiation patterns that are; almost omnidirectional in the H-plane, and like monopole pattern in the E-plane. The simulation results are analyzed and compared with measured results for verification.

1. INTRODUCTION

During the last decade, enormous advancements in designing wireless systems have been achieved. The portable devices in the market are offering many advantages like the small size, low cost and the support of many applications like Bluetooth, internet service, making calls and GPS services. Variety of applications, which are working on designated frequency bands, need antennas operating on these bands to be mounted in the same device. The use of more than one antenna in the same device is not a practical solution, because of the limited size in the new wireless devices. Therefore, various antennas working on dual or multi bands have been developed by the researchers over the years.

Taking the benefits of utilizing the self similarity property of fractal shapes a dual band fractal monopole was proposed by [1, 2]. The use of slot structures to achieve multi-band characteristics was proposed in [3–5]. The use of ring shaped antenna to operate on dual

* Corresponding author: Khalil Hassan Sayidmarie (kh.sayidmarie@gmail.com).

band was proposed by [6, 7]. Many other planar monopole antennas and microstrip antennas were proposed to operate on dual or multi band fashion [8–11].

In this contribution, three dual band planar monopole antennas for wireless local area network (WLAN) application are proposed. The antennas have self-similar double ring configurations in the form of rectangular, rhombic and annular rings. The proposed antennas which cover the frequency bands of the IEEE 802.11 a/b/g (2.4–2.48 GHz, 5.15–5.35 GHz and 5.725–5.825 GHz), are investigated using CST and HFSS software packages, and the obtained results are discussed and validated by experimental measurements.

2. ANTENNA DESIGN

The self similarity property of the fractal geometry is utilized to design the dual band monopole antennas. To implement the self similarity principle each antenna is formed of two similar in-shape rings, where the inner ring is a scaled copy of the outer one. The dimensions of the two rings were initially chosen such that the mean circumference of each ring corresponds to the effective wavelength at the center of the wanted frequency band. Thus, the outer ring corresponds to the lower band while the inner one corresponds to the upper band. The dimensions can then be slightly changed or optimized to get better response using a software package. The three antennas were constructed on the FR-4 substrate with a dielectric constant of 4.4, thickness of 1.6 mm, and tangent loss of 0.025. The width of the feed line for each antenna was fixed at 3.2 mm to implement 50 Ohm characteristic impedance of the SMA connector, and the length of the feed was put at $L_f = 17$ mm to represent a $\lambda/4$ transformer at the lower band. The CST software package was used to assess the characteristics of the three antennas. Further validations were achieved by using the HFSS software package.

2.1. Dual Rectangular Ring Antenna

The geometry of the first proposed antenna is shown in Fig. 1. The dual rectangular ring radiating patch and the microstrip feed line are etched on the same surface of the substrate, and the tapered rectangular ground, is put on the opposite surface of the substrate. The parameters of this antenna are shown in Table 1.

The investigations start with assessing the effect of tapering the ground plane by cutting two triangles from the upper corners of the ground plane as shown in Fig. 1(c). The return loss characteristics for various values of the height (U) of the cut triangles are shown in

Table 1. Parameters of the dual rectangular ring antenna. All dimensions are in millimeters.

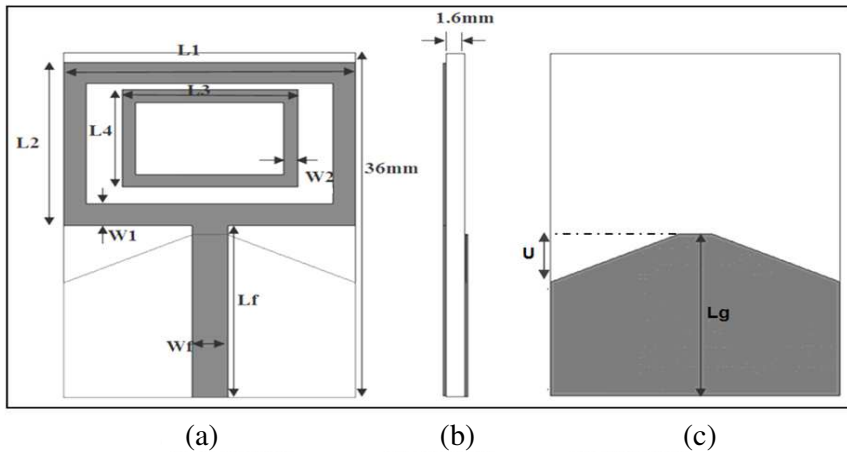| L_1	L_2	L_3	L_4	W_1	W_2	L_f	W_f	L_g	U
26	17	15.6	10.2	2.25	1.4	18	3.2	17	5

Figure 1. Geometry of the dual rectangular ring antenna. (a) Front view. (b) Side view. (c) Back view.

Fig. 2. It can be seen that the taper has little effect on the lower frequency band as exhibited by the slight shift in its center frequency, while the tapering increases the width of the second band. Values of the parameter (U) larger than 5 mm were found to decrease the bandwidth and produce inferior response. The tapering results in an increase in the separation between ground plane and lower side of the outer ring, thus allowing better current distribution along this edge.

After choosing the tapered ground plane with ($U = 5$ mm), the return loss results of the rectangular double ring antenna were verified by running another simulation using the HFSS software package, and the obtained results are shown in Fig. 3. It can be seen that the results obtained from the two software packages have good agreement. The same figure shows the return loss results when only the outer ring is considered and using both software packages. It can be seen that the first resonance is at a frequency of 2.7 GHz, and a second mode, with lower matching, at about 5.3 GHz. The ratio of the two frequencies is 1.963 or about 2 corresponding to cases where the ring circumference equals one and two wavelengths respectively. With the use of two rings,
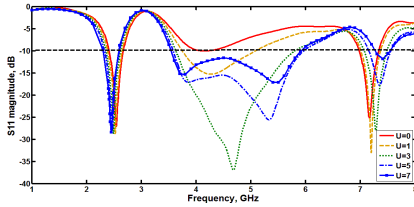
Figure 2. Return loss of the dual rectangular ring antenna showing effects of tapering the ground plane. The height (U) of the cut triangles is shown in Fig. 1.
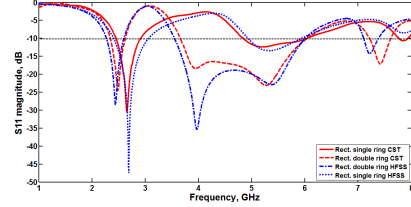
Figure 3. Return loss of the dual rectangular ring antenna compared to that of the same antenna without the inner ring, as obtained from CST and HFSS software packages, for $U = 5\,\mathrm{mm}$.
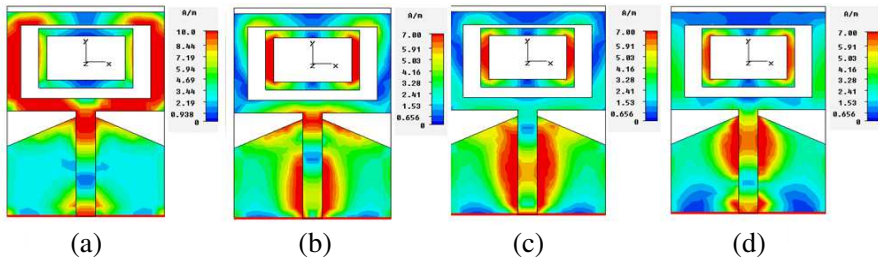

Figure 4. Surface current distributions of the dual rectangular ring antenna as obtained from the CST software, at the indicated frequencies. (a) 2.47 GHz. (b) 4 GHz. (c) 5.2 GHz. (d) 5.5 GHz.

the second resonance can be selected by varying the inner/outer ring size ratio. In such a case, the resonance due to the inner ring and the second resonance due to the outer ring combine together to form wider band, which is evident in Fig. 3.

For better insight into the dual band operation of the antenna, the surface current distribution across the rings was found using the CST software. The obtained current distributions at four selected frequencies are shown in Fig. 4. It can be seen that, at the lower frequency band the outer ring has rich current distribution, while at the upper frequency band the inner ring has richer surface current. This indicates that the outer ring controls the lower band frequency, while the inner ring influences the upper band frequency. Moreover, the inner band almost preserve its current density at frequencies of 4, 5.2, and 5.5 GHz indicating the wider upper band.

The frequency characteristics of the dual rectangular ring antenna,

Table 2. Frequency characteristics of the dual rectangular ring antenna, for $U = 5$ mm.

Software	$F1$ (GHz)	$BW1$ (GHz)	Mean circumference of the outer ring (mm)	λ_{d1} (mm) Eq. (2)	λ_{d1} /mean circum. (Eq. (2))
CST	2.48	2.34–2.61	77	73.61	0.955
HFSS	2.44	2.27–2.59	77	74.82	0.971
Software	$F2$ (GHz)	$BW2$ (GHz)	Mean circumference of the inner ring (mm)	λ_{d2} (mm) Eq. (2)	λ_{d2} /mean circum. (Eq. (2))
CST	4.83	3.66–6	46	37.8	0.821
HFSS	4.77	3.55–6	46	38.27	0.831

for $U = 5$ mm, were derived from the obtained return loss results, and are shown in Table 2. The two software packages show similar bands with little differences. The effective wavelength λ_d in the substrate was calculated using the formula [12]:

$$\lambda_d = \lambda_o / \sqrt{\varepsilon_e} \tag{1}$$

where λ_o is the wavelength in air, and ε_e is the effective relative dielectric constant given by [7, 11]:

$$\epsilon_e = \frac{\epsilon_r + 1}{2} \tag{2}$$

Formula (2) is mostly used in monopole designs, while the following formula (3) has been used for microstrip antenna design [12]. Formula (3) was used to calculate the impedance value of the feed line.

$$\epsilon_e = \frac{\varepsilon_r + 1}{2} + \frac{\varepsilon_r - 1}{2} \left(1 + 12 \frac{h}{w} \right)^{-1/2} \tag{3}$$

For the used FR4 substrate, the obtained value of ε_e from Eq. (2) equals 2.7. Referring to Fig. 1, the mean circumferences C_{or}, and C_{ir} of outer and inner rings respectively can be calculated as:

$$C_{or} = 2(L_1 + L_2) - 4W_1 \tag{4}$$
$$C_{ir} = 2(L_3 + L_4) - 4W_2 \tag{5}$$

It can be seen from Table 2 that the ratio of wavelength λ_{d1} in the substrate to the mean circumference of the outer ring is 0.955

for the first band whose center frequency is at 2.48 GHz. The ratio
for the inner ring was found to be 0.821, at the considered center
frequency of 4.83 GHz. These results indicate a good relation between
the circumferences of the rings and effective wavelength. Moreover,
with such relations one can choose the dimensions of the ring from the
center frequency of each of the two bands at the design stage.

2.2. Dual Rhombus Ring Antenna

The geometry of the second proposed antenna is shown in Fig. 5.
The dual rhombic ring radiating patch and its microstrip feed line
are etched on one side of the substrate, while the tapered rectangular
ground is on the opposite side of the substrate. The parameters of the
second antenna are shown in Table 3.

The effect of tapering the ground plane by cutting two triangles
from the upper corners of the ground plane was investigated. The
return loss characteristics for various values of the height (U) of the
cut triangles are shown in Fig. 6. It can be seen that the taper has
little effect on the frequency of the first band as it shifts the center
frequency slightly to lower values. The tapering has made the second
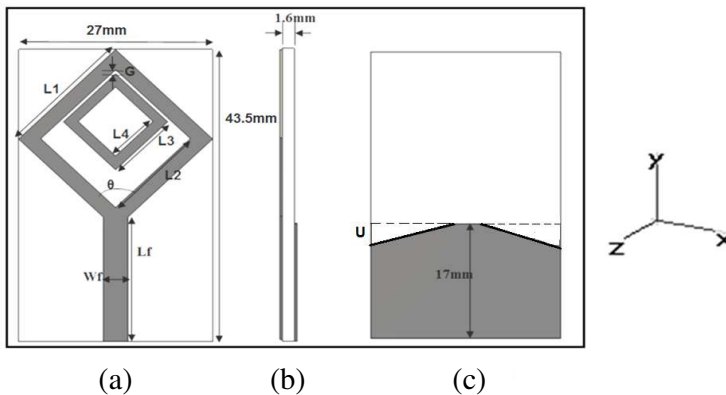band narrower and of less matching characteristics. The reason for this

Figure 5. Geometry of the dual rhombic ring antenna. (a) Front
view. (b) Side view. (c) Back view.

Table 3. Parameters of the dual rhombic ring antenna. All dimensions
are in millimeters.

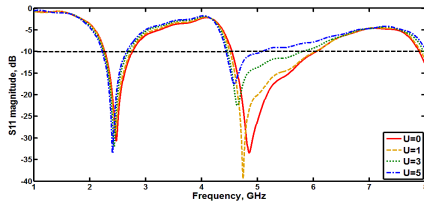| L_1	L_2	L_3	L_4	L_f	W_f	Θ (degree)	G
19	14.8	10.6	7	18	3.2	90	0.5

Figure 6. Return loss curves of the dual rhombic antenna showing the effect of tapering the ground plane. The height (U) of the cut triangles is shown in Fig. 5.
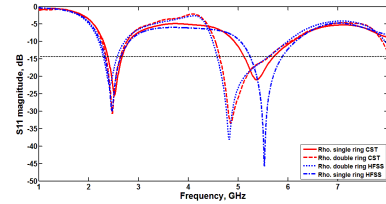
Figure 7. Return loss of the dual rhombic ring antenna compared to that of the same antenna without the inner ring, as obtained from CST and HFSS software packages, for $U = 0\,\mathrm{mm}$.

effect can be attributed to the fact that the rhombic shape inherently produces triangular spacing between the edges of the ground plane and the lower sides of the outer ring. Such spacing is needed for the case of the rectangular ring antenna, and was achieved by tapering the ground plane. An inverse tapering, by adding two triangles instead of cutting them, was investigated but it gave inferior results.

After choosing the ground plane shape without tapering ($U = 0$), the return loss results of the dual rhombic ring antenna were verified by running another simulation using the HFSS software package, and the obtained results are shown in Fig. 7, indicating very good agreement. The same figure shows the return loss results when only the outer ring is considered and using both software packages. It can be seen that there is a deep null at a frequency of 2.52 GHz, and a second mode resonance at about 5.52 GHz, indicating a frequency ratio of 2.12 or about 2. This behavior is similar to that seen for the dual rectangular ring antenna discussed in Section 2.1.

The current distribution across the surface was found using the CST software to have further insight into the dual band operation of the antenna. The obtained surface current distributions at three selected frequencies are shown in Fig. 8. It can be seen that at the lower band frequency of 2.5 GHz the outer ring has rich current distribution, while at the upper band frequency the inner ring has a larger surface current. At a frequency of 5.5 GHz the inner ring current decreases in favor of that for the outer ring. These results also indicate that the outer ring corresponds to the lower frequency band, while the inner ring controls the frequency of the upper band.

Detailed frequency characteristics of the dual rhombic antenna, for $U = 0\,\mathrm{mm}$, were derived from the obtained return loss results, and

(a)   (b)   (c)
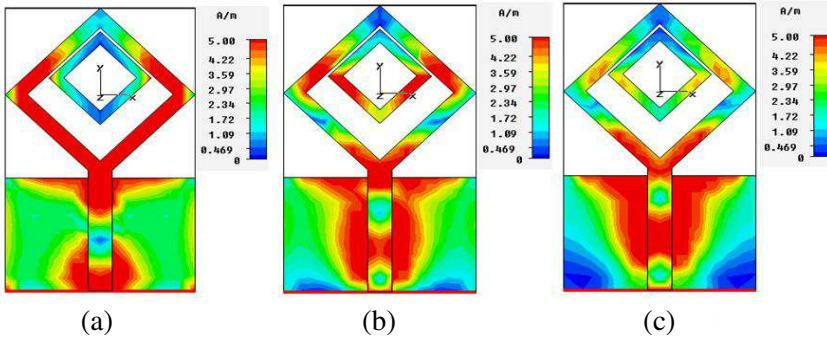
Figure 8. Surface current distributions of the dual rhombic ring antenna as obtained from the CST software, at the shown frequencies. (a) 2.5 GHz. (b) 5 GHz. (c) 5.5 GHz.

Table 4. Frequency characteristics of the dual rhombus ring antenna, for $U = 0$ mm.

Software	$F1$ GHz	$BW1$ GHz	Mean circumference of outer ring (mm)	λ_{d1} (mm) Eq. (2)	λ_{d1} /mean circum. Eq. (2)
CST	2.47	2.27–2.76	67.6	73.91	1.093
HFSS	2.42	2.2–2.72	67.6	75.44	1.115
Software	$F2$ GHz	$BW2$ GHz	Mean circumference of inner ring (mm)	λ_{d2} (mm) Eq. (2)	λ_{d2} /mean circum. Eq. (2)
CST	5.27	4.54–6	35.2	34.64	0.984
HFSS	5.25	4.5–6	35.2	34.77	0.987

are listed in Table 4. Referring to Fig. 5, the mean circumferences C_{orh} and C_{irh} of outer and inner rings respectively were calculated from:

$$C_{orh} = 2(L_1 + L_2) \qquad (6)$$
$$C_{irh} = 2(L_3 + L_4) \qquad (7)$$

It can be seen that the ratio of wavelength λ_{d1} in the substrate (using Eqs. (1)&(2)) to the mean circumference of the outer ring is 1.093 for the first band whose center frequency is at 2.47 GHz. The same ratio for the inner ring was found to be 0.984, at the considered center frequency of 5.27 GHz. These results indicate the strong correspondence between the circumferences of the rings and wavelength in the substrate.
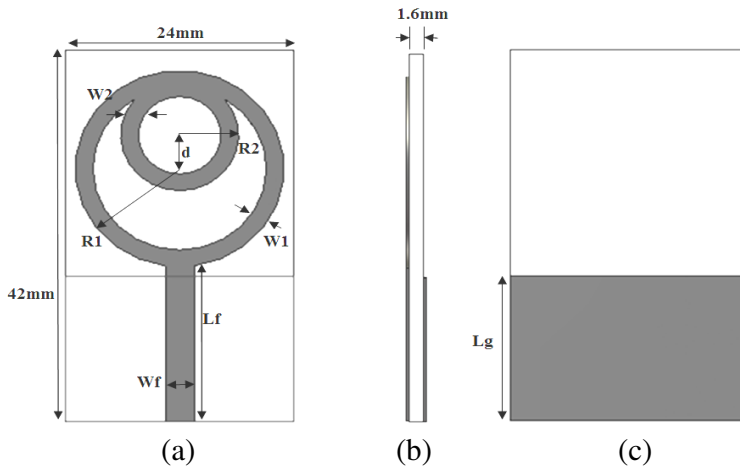
Figure 9. Geometry of the dual annular ring antenna. (a) Front view. (b) Side view. (c) Back view.

Table 5. Parameters of the dual annular ring antenna. All dimensions are in millimeters.

R_1	R_2	W_1	W_2	L_f	W_f	L_g	d
11.5	6.5	2	2	18	3.2	17	4

2.3. Dual Annular Ring Antenna

The geometry of the third proposed antenna is shown in Fig. 9. The dual annular ring radiating patch and the microstrip feed line are etched on the same surface of the substrate, while the rectangular ground plane is on the opposite surface of the substrate. Detailed parameters of the third antenna design are shown in Table 5. The dimension d represents the separation between centers of the two rings. For this antenna, the inner ring is shifted from the center by 4 mm and combined with outer ring. The effect of locating the inner ring was investigated by assessing the return loss characteristics for the three locations shown in Fig. 10, and the obtained return loss responses are shown in Fig. 11. It is evident from the figure that when the inner ring was placed at the center of the outer ring the response is of lower quality. When the inner ring was combined with the upper side of the outer ring (case 3), better response was achieved. The frequency of the lower band decreased slightly while the upper band showed much improvement. The results can be attributed to the fact that the lower
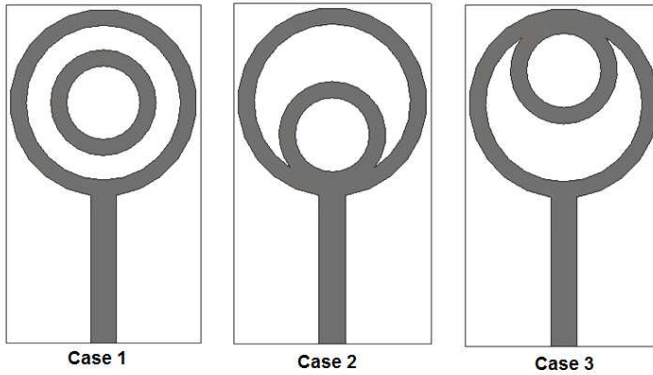
Figure 10. The investigated locations of the inner ring of the dual annular ring antenna.
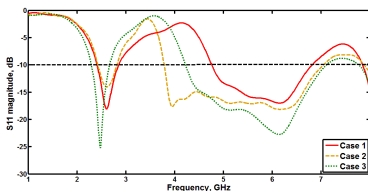

Figure 11. Return loss curves of the dual annular ring antenna for the three locations of the inner ring shown in Fig. 10.
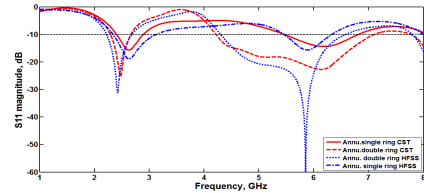
Figure 12. Return loss of the dual annular ring antenna compared to that of the same antenna without the inner ring, as obtained from CST and HFSS software packages, for $U = 0\,\text{mm}$.

part of the outer ring is richer in surface current as compared to the upper part. Therefore, the coupling between the two rings is different for the three cases.

The antenna having the inner ring location shown in case 3 was chosen, and its return loss results were verified by running another simulation using the HFSS software package, and the obtained results are shown in Fig. 12. The two software packages show good agreement. The same figure shows the return loss results when only the outer ring is considered and using both software packages. It can be seen that there is a deep null at a frequency of 2.62 GHz, and a second mode resonance at about 5.89 GHz. The ratio of the two frequencies is 2.24, which is slightly higher than those found with other two antennas.

With the use of two rings, the second resonance can be selected by varying the ratio of ring sizes. In such a case, the resonance due to the inner ring and the second resonance of the outer ring combine together to form wider band.

For further assessment of the dual band operation of the antenna, the current distributions on the surface of the rings were found using the CST software. The obtained surface current distributions at three selected frequencies are shown in Fig. 13. It can be seen that at the center of the lower frequency band of 2.47 GHz the outer ring has rich current distribution compared with the inner ring. At the upper frequency band the inner ring has a larger surface current. At a frequency of 5.2 GHz the inner ring current decreases slightly in favor
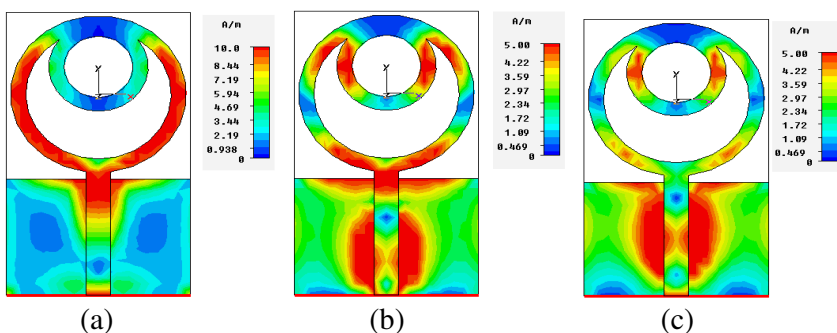

(a)   (b)   (c)

Figure 13. Surface current distributions of the dual annular ring antenna as obtained from the CST software, at the shown frequencies. (a) 2.47 GHz. (b) 4.8 GHz. (c) 5.2 GHz.

Table 6. Detailed frequency characteristics of the dual ring antenna at various radii of the rings.

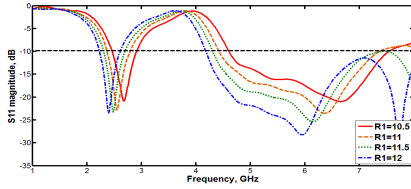| R_1	R_2	$F1$ (GHz)	$B.W.1$ (GHz)	$B.W.2$ (GHz)	λ_{d1}/mean circum.
10.5	6	2.68	2.46–2.91	4.6–7.5	1.141
11	6	2.55	2.37–2.78	4.42–7.36	1.139
11.5	6	2.48	2.3–2.69	4.31–7.29	1.115
12	6	2.4	2.23–2.6	4.18–8.13	1.100
R_1	R_2	$F1$ (GHz)	$B.W.1$ (GHz)	$B.W.2$ (GHz)	λ_{d2}/mean circum.
11.5	6.5	2.47	2.29–2.66	4.22–7.1	0.933
11.5	6	2.47	2.29–2.72	4.31–7.43	0.990
11.5	5.5	2.49	2.32–2.72	4.41–8.44	1.001
11.5	5	2.49	2.32–2.72	4.54–8.35	1.126

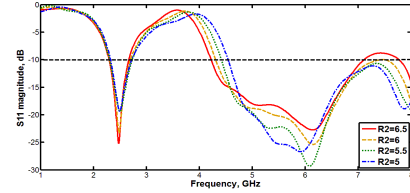**Figure 14.** Return loss curves for various radii of the outer ring, while the inner ring radius was kept constant at $R_2 = 6\,\text{mm}$.

Figure 15. Return loss curves for various radii of the inner ring, while the outer ring radius was kept constant at $R_1 = 11.5\,\text{mm}$.

of that for the outer ring. These results also indicate that the outer ring influences the lower frequency band, while the inner ring controls the upper frequency band.

To verify that the outer ring controls the frequency of the lower band, the inner ring radius was fixed at 6 mm, and the return loss results for various outer ring radii were found as shown in Fig. 14, and Table 6. It can be seen that as the ring radius is increased the return loss response shifts towards lower frequencies. The table shows that the ratio (λ_{d1}/mean circumference) is near to unity. By a similar procedure, the outer ring radius was fixed at 11.5 mm, and the return loss results for various inner ring radii were found as shown in Fig. 15, and Table 6. It can be seen that as the ring radius is increased the return loss response shifts slightly towards lower frequencies. The table shows that the ratio (λ_{d2}/mean circumference) is around unity.

Detailed frequency characteristics of the dual annular ring antenna were derived from the obtained return loss results, and are listed in Table 7. It can be seen that the ratio of wavelength λ_{d1} in the substrate (using Eqs. (1)&(2)) to the mean circumference of the outer ring is 1.12 for the lower band whose center frequency is at 2.47 GHz. The same ratio for the inner ring was found to be 0.944, at the considered center frequency of 5.6 GHz. These results indicate a good relation between the circumferences of the rings and effective wavelength at the frequency of resonance.

3. EXPERIMENTAL VALIDATIONS

The simulated results for the three antennas were verified by the experimental results. The three antennas were fabricated using the same substrate and design parameters used in the simulations and listed Tables 1, 3, and 5. A CNC PCB cutting machine was used in

Table 7. Frequency characteristics of the dual annular ring antenna.

Software	$F1$ GHz	$BW1$ GHz	Mean circumference of outer ring (mm)	λ_{d1} (mm) Eq. (2)	λ_{d1} /mean circum.
CST	2.47	2.29–2.66	65.97	73.91	1.120
HFSS	2.41	2.2–2.7	65.97	75.75	1.148
Software	$F2$ GHz	$BW2$ GHz	Mean circumference of inner ring (mm)	λ_{d2} (mm) Eq. (2)	λ_{d2} /mean circum.
CST	5.6	4.22–7.1	34.5	32.6	0.944
HFSS	5.3	4.15–6.6	34.5	34.44	0.998
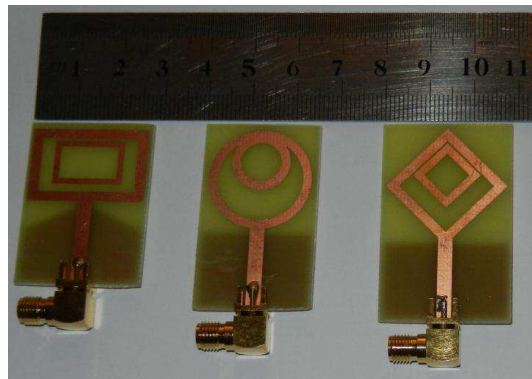
Figure 16. The double ring antennas printed on FR4 substrate.

the fabrication, and the fabricated antennas are shown in Fig. 16. The experimental tests for the three antennas were performed using Rode and Schwarz ZVL13 vector network analyzer (VNA) to measure the return loss over the frequency range of 1–8 GHz. The measured return loss S_{11} data set comprised 201 discrete data points in magnitude $|S_{11}|$ and phase $\arg(S_{11})$, which were exported to a USB memory through the VNA port for plotting by computer. Fig. 17 shows the experimental return loss response of the double rectangular ring antenna compared to the responses obtained from CST and HFSS simulations. The experimental response fairly compares to the simulation results in general, while the first band shows good correspondence.

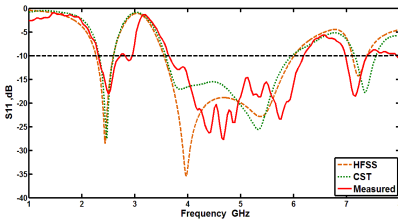Figure 18 shows the experimental return loss response of the

Figure 17. Return loss responses for double ring rectangular antenna obtained from measurement and simulations.
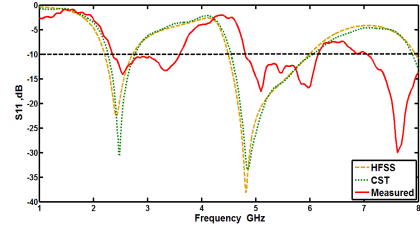

Figure 18. Return loss responses for double rhombic ring antenna obtained from measurement and simulations.
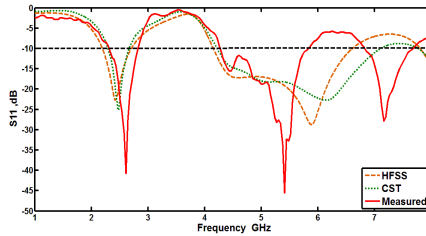

Figure 19. Return loss responses for double annular ring antenna obtained from measurement and simulations.

double rhombic ring antenna compared to the responses obtained from simulations. The experimental response fairly compares to the simulation results in general, the first band shows good correspondence, while the upper band shows lower width. Fig. 19 shows the experimental return loss response of the double annular ring antenna compared to the responses obtained from CST and HFSS simulations. The experimental response shows better agreement with the simulation results in general, the first band shows good correspondence, while the upper band shows lower width.

The far field patterns of the three proposed antennas were measured in an anechoic chamber at three different frequencies and the obtained results are compared with simulation ones as shown in Figs. 20–22. It can be seen that the antennas preserve their omnidirectional patterns in the XZ plane at the two bands. The patterns in the XY plane show typical dipole pattern. Good agreement is noticed between simulation and measured results.

The gain values of the three proposed antennas were calculated from the far field patterns using the HFSS package, and the obtained results are shown in Fig. 23. The gain has the general trend of increasing with frequency except between the two bands, where there is a dip of about 1 dB.
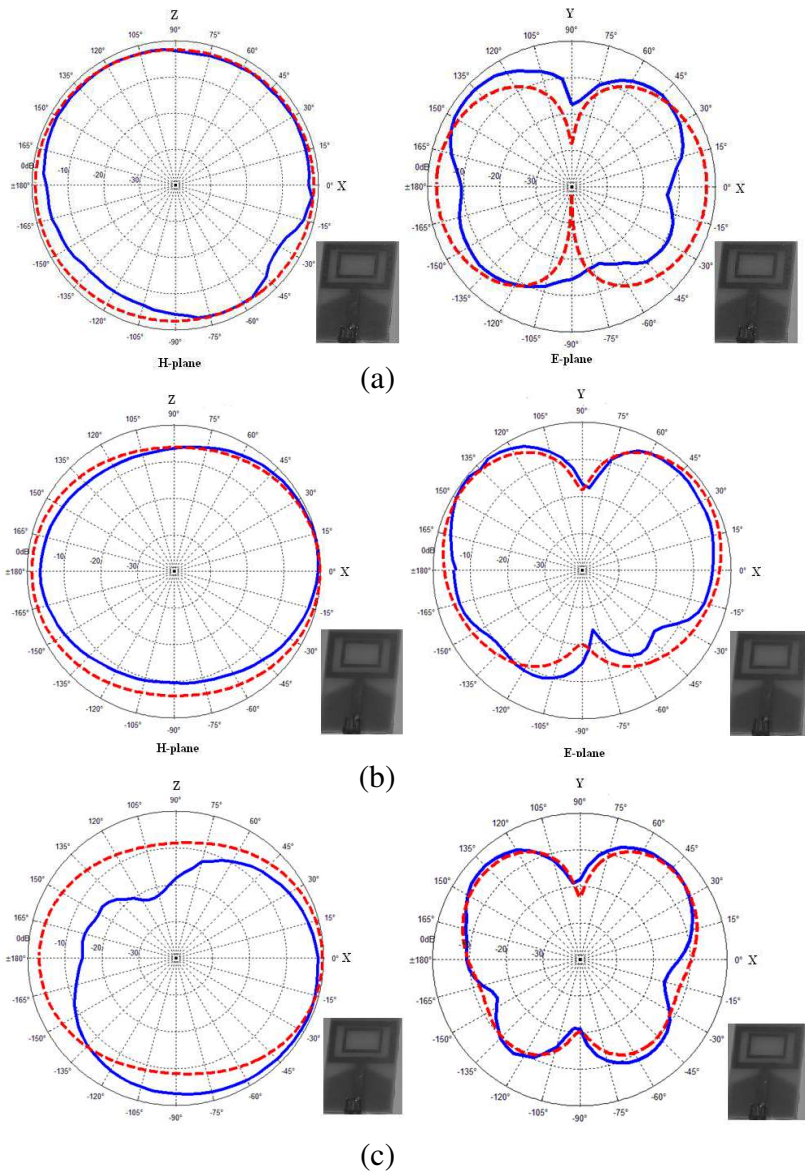
Figure 20. The simulated and measured radiation patterns of the dual rectangular ring antenna; (a) at 2.45 GHz, (b) at 5.25 GHz, (c) at 5.75 GHz, '—' measured, '- - -' simulation using CST.
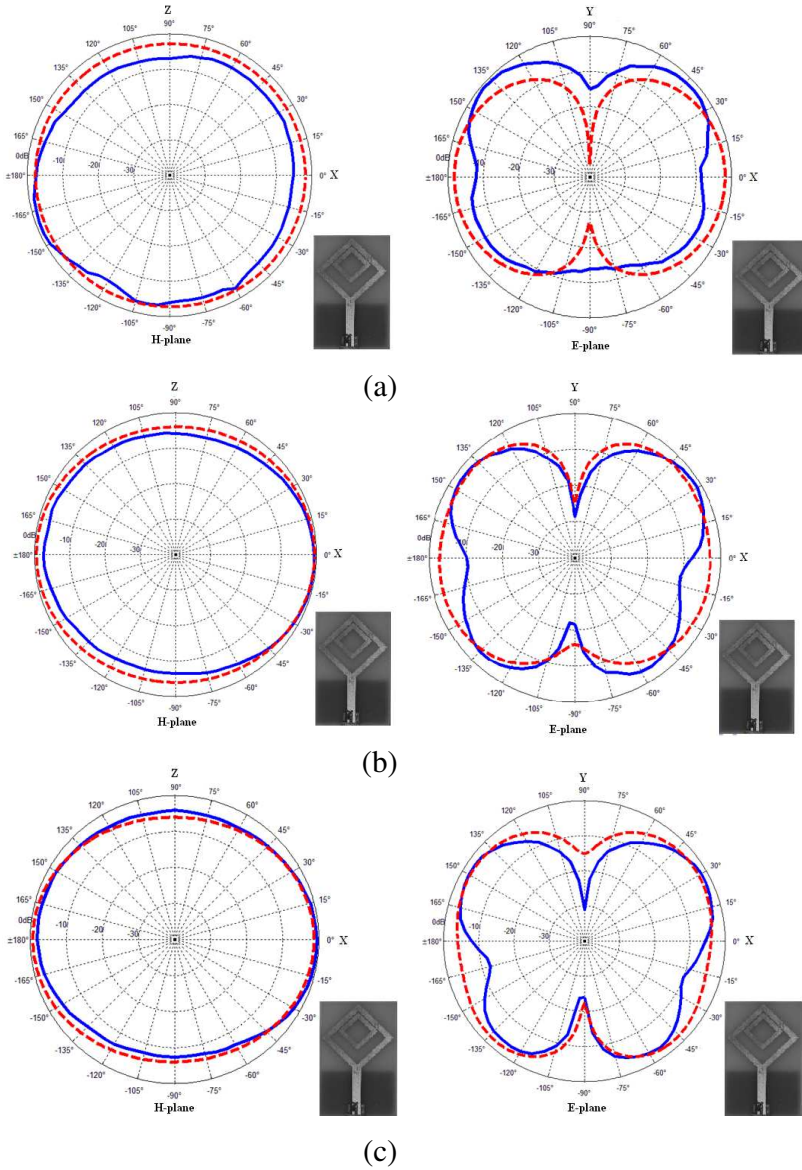
(a)

(b)

(c)

Figure 21. The simulated and measured radiation patterns of the dual rhombic ring antenna; (a) at 2.45 GHz, (b) at 5.25 GHz, (c) at 5.75 GHz , '—' measured, '- - -' simulation using CST.
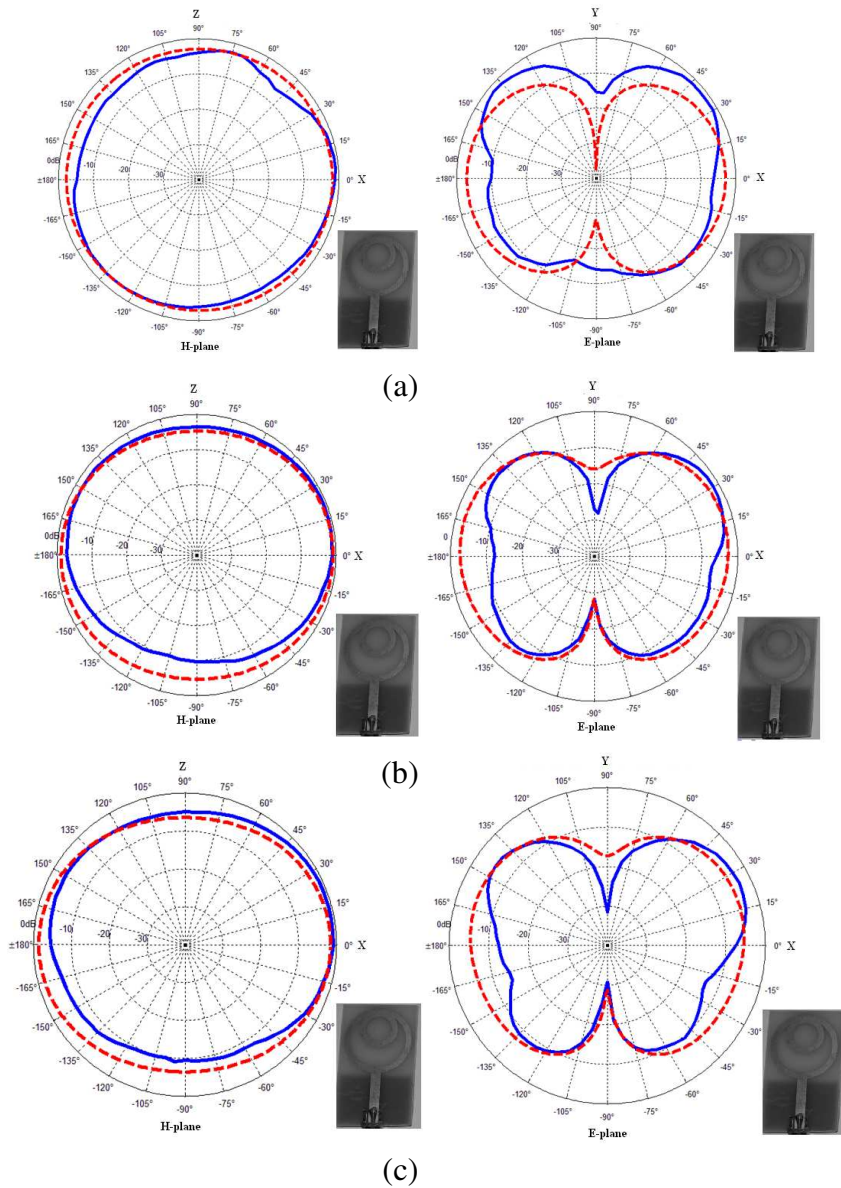
(a)

(b)

(c)

Figure 22. The simulated and measured radiation patterns of the dual annular ring antenna; (a) at 2.45 GHz, (b) at 5.25 GHz, (c) at 5.75 GHz , '—' measured, '---' simulation using CST.
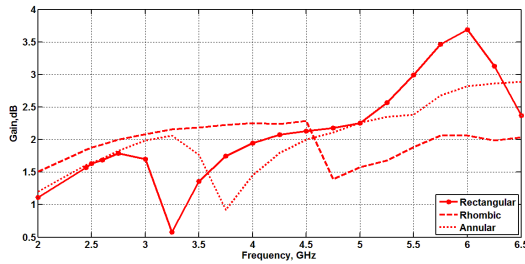
Figure 23. Variation of calculated gain with frequency for the three proposed antennas.

4. CONCLUSIONS

The design and analysis of three dual band planar monopole antennas for wireless local area network (WLAN) application has been demonstrated. The antennas have common configuration of rectangular, rhombic and annular double rings. All the antennas use the self similarity property to exhibit dual band characteristics. The proposed antennas showed compact dimensions of less than 0.22×0.36 of the free space wavelength at the lower band. The circumference of the outer ring controls the lower band frequency, while the upper band is mainly influenced by the inner ring. The results showed that the lower band is more precisely governed by the outer ring since, at the lower band the inner ring is far from resonance. The inner ring has relatively less effect on the upper band, as it shares the effect with the outer ring which can be at second mode resonance at this band. This can also be attributed to the mutual coupling effect on the inner ring. When the inner ring is in resonance, the outer ring can be in resonance at higher mode (double frequency) if the upper band frequency is twice that of the lower band. The experimental results showed acceptable agreement with the simulation results. The measured radiation patterns showed good agreement with the simulation results.

REFERENCES

1. Asis, R. S., M. A. Alkanhal, and A. F. Sheta, "Dual band fractal monopoles," *Saudi International Conference on Electronics, Communications and Photonics (SIECPC)*, 1–5, April 24–26, 2011.

2. Lizzi, L. and A. Massa, "Dual-band printed fractal monopole antenna for LTE applications," *IEEE Transaction on Antennas*

and Wireless Propagation Letters, Vol. 10, 760–763, August 8, 2011.

3. Kang, L., Y.-Z. Yin, S.-T. Fan, and S.-J. Wei, "A novel rectangular slot antenna with embedded self-similar T-shaped strips for WLAN applications," *Progress In Electromagnetics Research Letters*, Vol. 15, 19–26, 2010.

4. Zhong, S.-S. and X.-L. Liang, "Dual-band printed T-shaped slot antenna for WLAN application," *Asia-Pacific Microwave Conference, APMC*, 1730–1734, December 12–15, 2006.

5. Wei, Y., Y. Yin, Y. Jing, and W. Hu, "Compact dual-band antenna with modified open U-shaped slot for WLAN applications," *IEEE International Conference on Microwave Technology & Computational Electromagnetics (ICMTCE)*, 35–37, International Convention Center Beijing, China, May 22–25, 2011.

6. Yang, B., Y. C. Jiao, W. Zhang, H. Xie, and F. S. Zhang, "Dual-band ring-shaped antenna for WiMAX/WLAN applications," *IEEE International Conference on Microwave Technology & Computational Electromagnetics (ICMTCE)*, 38–40, International Convention Center Beijing, China, May 22–25, 2011.

7. Behera, S. and K. J. Vinoy, "Microstrip square ring antenna for dual-band operation," *Progress In Electromagnetics Research*, Vol. 93, 41–56, 2009.

8. Liu, L., S. Zhu, and R. Langley, "Dual-band triangular patch antenna with modified ground plane," *Electronics Letters*, Vol. 43, 140–141, February 1, 2007.

9. Mishra, S. K., R. Gupta, A. Vaidya, and J. Mukherjee, "Printed fork shaped dual band monopole antenna for Bluetooth and UWB applications with 5.5 GHz WLAN band notched characteristics," *Progress In Electromagnetics Research C*, Vol. 22, 195–210, 2011.

10. Alkanhal, M. A., "Composite compact triple-band microstrip antennas," *Progress In Electromagnetics Research*, Vol. 93, 221–236, 2009.

11. Xiong, L. and P. Gao, "Dual-band planar monopole antenna for bluetooth and UWB applications with WiMAX and WLAN band-notched," *Progress In Electromagnetics Research Letters*, Vol. 28, 183–194, 2012.

12. Kumar, G. and K. P. Ray, *Broad Band Microstrip Antenna*, Artech House, 2003.